Experimental Characterization of a Solid Oxide Fuel Cell Coupled to a Steam-Driven Micro Anode Off-Gas Recirculation Fan

Patrick Hubert Wagner[a], Zacharie Wuillemin[b,c], David Constantin[b], Stefan Diethelm[b,c], Jan Van herle[b], Jürg Schiffmann[a,*]

[a] *Laboratory for Applied Mechanical Design (LAMD), Institute of Mechanical Engineering (IGM), Ecole Polytechnique Fédérale de Lausanne (EPFL), Neuchâtel, 2000, Switzerland*
[b] *Group of Energy Materials (GEM), IGM, EPFL, Sion, 1951, Switzerland*
[c] *SOLIDpower SA, Yverdons-les-Bains, 1400, Switzerland*

Abstract

While the global fuel utilization (FU) of solid oxide fuel cells (SOFCs) is limited by the stack aging rate, the fuel excess is typically used in a burner, and thus limiting the system electrical efficiency. Further, natural-gas-fueled SOFCs require treated water for the steam reforming process, which increases operational cost.

Here, we introduce a novel micro anode off-gas recirculation (AOR) fan that is driven by a partial-admission (21 %) and low-reaction (13 %) steam turbine with a tip diameter of 15 mm. The 36 W turbine is propelled by pressurized steam, which is generated from the excess stack heat. The shaft runs on dynamic steam-lubricated bearings and rotates up to 175 krpm.

For a global FU of 75 % and a constant fuel mass flow rate, the electrical gross DC efficiency based on the lower heating value (LHV) was improved from 52 % to 57 % with the AOR, while the local FU decreased from 75 % to

*Corresponding author. E-mail address: jurg.schiffmann@epfl.ch

61 %, which is expected to significantly increase stack lifetime. For a global FU of 85 %, gross efficiencies of 66 % in part load (4.5 kW_{el}) and 61 % in full load (6.3 kW_{el}) were achieved with the AOR. The results suggest that the steam-driven AOR can achieve a neutral water consumption.
Keywords: solid oxide fuel cell, anode off-gas recirculation, small-scale turbomachinery, radial fan, steam turbine, gas bearings

1. Introduction

The combination of steam-reforming solid oxide fuel cell (SOFC) systems with anode off-gas recirculation (AOR) leads (1) to higher efficiency due to higher global fuel utilization (FU), (2) to higher life time due to lower local FU, and (3) to water-neutral operation, i.e., without water supply and treatment. A recirculation unit is needed to overcome the pressure loss of the SOFC stack, reformer, heat exchangers, and piping. Besides fuel and steam-driven ejectors, recirculation fans are commonly used. The literature provides several examples of realizations of SOFC systems with electrically-driven AOR fans. Within this section, all mentioned power ratings are stated as gross DC power and the all mentioned efficiencies are stated as electrical gross DC efficiencies based on the fuel lower heating value (LHV).

Powell et al. [1] experimentally demonstrated the technical feasibility of a planar SOFC system with AOR. They reported a power output between 1.9 kW_{el} and 2.6 kW_{el}, reaching efficiencies of 63 % and 57 %, for a global FU of 93 % and 86 %, respectively. According to the authors, an oversized AOR fan was used for their tests, since no adequate fan was available off-

the-shelve.

Borglum and Ghezel-Ayaghy [2] tested a 59 kW_{el} SOFC system with an "anode recycle blower". The stack was composed of planar cells and was operated at ambient pressure. An electrical efficiency of 64 % for a global FU of 81 % was reached.

Halinen et al. [3] operated a 10 kW_{el} planar cross-flow SOFC with 66 % efficiency over 10 000 h. A 100 W_{el} "high-temperature recycle blower" was used for the AOR.

Peters et al. [4] operated a planar SOFC stack at 2.5 kW_{el} and 4 kW_{el} with AOR, reaching efficiencies of 64 % and 60.5 %, respectively for a global FU of 90 %. They claim that if a new stack had been used instead of an aged one, the efficiency would have been at least five percentage points higher. An electrically-driven side channel blower with a magnetic coupling was used.

More recently, Bosch announced a plug and play 10 kW_{el} SOFC equipped with AOR, reaching an efficiency of 70 %. Unfortunately, no details on the AOR unit were published [5].

Besides rolling-element-supported AOR fans that are coupled to the electric motor with a magnetic coupling [1, 4], literature also provides examples of directly coupled fans on ball bearings [6], dynamic oil film bearings [7], or dynamic gas film bearings. The latter option has the advantage of oil-free operation, resilience to high temperatures, and a long life time, which makes this concept particularly interesting for SOFC systems. Current designs [8, 9] use gas foil journal and thrust bearings.

Wagner et al. [10] presented the design of a novel AOR fan supported on

herringbone-grooved journal and spiral-grooved thrust gas film bearings. Due to the relatively low AOR mass flow rate and relatively high fan pressure rise for a 10 kW_{el} SOFC system, the fan has a tip diameter of only 19.2 mm and rotates up to 175 krpm. Prior to coupling this AOR fan with an SOFC system, the fan was experimentally characterized with air at 200 °C. At nominal operation of 168 krpm, the measured inlet mass flow rate was 4.9 $kg\,h^{-1}$, reaching a total-to-total pressure rise of 55 mbar, and an isentropic total-to-total efficiency 55 %, yielding a power of 18.3 W.

The objective of this paper is thus to couple this AOR fan to an SOFC stack and to demonstrate the feasibility of such a system. Both SOFC stack with the AOR fan and without AOR are characterized.

2. SOFC system with thermally-driven AOR fan

The previously mentioned AOR fan concept introduced by Wagner et al. [10] was coupled to a 6 kW_{el} SOFC system. Instead of using an electrically-driven AOR fan, the new AOR concept is propelled by a 15 mm tip diameter, partial-admission (21 %), and low-reaction (13 %) steam turbine [11]. Figure 1 a) shows the rotor the fan-turbine unit (FTU). On the left side is the radial AOR fan and on the right side the radial-inflow steam turbine. Both the fan and turbine impeller are directly coupled with the gas-bearing-supported rotor that is coated with diamond-like carbon (DLC). The V-shapes on the rotor indicate the positions of the herringbone grooved journal bearings. The entire unit is manufactured with turning, milling, and surface finishing operations, i.e., grinding and honing. Since no electrical components are used in

the FTU, it is explosion-proof. Additionally, heat cogeneration in the SOFC system is used to propel the AOR fan, which increases the SOFC system electrical net efficiency.

Figure 2 gives a schematic overview of this novel SOFC system with the thermally-driven AOR fan. Both the SOFC and the FTU are in the same hot box. At the nominal operating point, natural gas is injected (stream 1 in Figure 2). The fuel is mixed with the recirculated anode off-gas (stream 7) that contains mainly deionized and neutral water vapor, carbon dioxide, and non-reacted hydrogen. Within the steam reformer, the fuel reacts with the water vapor to hydrogen and carbon dioxide. Part of the fuel can be reformed inside the stack (internal reforming) for maximization of the system net efficiency, since the endothermic steam reforming reaction cools the stack, and thus reduces the auxiliary electric power of the cathode fan (stream 31) [12]. The planar co-flow SOFC stack anode is fueled with hydrogen at 710 °C (stream 3). The air at the cathode inlet has a similar temperature of 710 °C. The heat exchanger (HEX) for heating the air (stream 24) to 710 °C is not shown in Figure 2. The anode off-gas (stream 4) has a temperature on the order of 800 °C; it is split into one part (stream 8) that is burned and another part (stream 5) that is recirculated to the steam reformer and to the anode inlet. Wagner et al. [10] suggested that a cold AOR leads to 0.5 percentage points higher electrical net efficiency compared to hot AOR, for the case of a 10 kW_{el} system with a conventional electrically-driven AOR fan. Since the system efficiency with cold AOR is expected to be higher and the FTU design is less complicated, a recirculation temperature of 200 °C was chosen for this proof-of-concept. However, this design needs an additional HEX at stream

4 and/or 5 to cool the anode off-gas from 800 °C to 200 °C. This leads to increased system cost and increased heat losses on the one hand, but increases the electrical net efficiency and mitigates the operational risk of the AOR fan on the other. The temperature difference between the steam turbine and the AOR fan should be low to avoid the risk of a bearing failure, since the nominal clearance between the rotating shaft and the non-rotating journal bearings is only a few micrometers; a too high differential thermal expansion between the journal bearing and the rotor could lead to a potential failure. For the first steam-driven AOR fan prototype, it was decided to maintain the mean fan temperature (stream 5 and stream 6) on the same order as the mean steam turbine temperature (stream 18 and 19), which results in a turbine inlet temperature (stream 18) of 220 °C. This limits the turbine power and efficiency, but allows for a safe operation of the FTU.

The FTU was designed in such that neither external water, nor external heat is necessary at nominal operation. Heat can be recovered internally with a HEX downstream of the burner. This HEX can provide heat to the anode preheating (stream 2), steam reformer, and evaporator. Uncondensed water vapor, unused hydrogen, and potentially-unreformed carbon monoxide (stream 8) is burned. A fan draws ambient air (stream 26) to the burner (stream 27) to control the flame temperature, and thus the burner outlet temperature (stream 10). The burner off-gas (stream 11) is cooled and partially condensed and exits to the chimney at a temperature of 60 °C (stream 9). Water can be recovered internally from the anode off-gas (stream 11) for a water-neutral operation, i.e., the mass flow rate in stream 14 is zero. Excess water exits the system at stream 13. The pressure of the remaining water

is increased by a pump to compensate the pressure loss in the evaporator and the turbine expansion; the total pressure at the turbine inlet (stream 18) is on the order of 2 bar. The water vapor is preheated, evaporated, and superheated, so that the turbine inlet total temperature is on the order of 220 °C. Part of the expanded steam (stream 20) is fed back to the condenser and another part (stream 21) exits the system through a chimney (or can be condensed).

3. Test rig setup

In order to simplify the control and the operation of the complete coupled system, the realized proof-of-concept (Figure 3) has several differences to the previously described concept of an SOFC system with a thermally-driven AOR fan (Figure 2). This leads, among other things, to a limitation of the electrical net efficiency and the utilization ratio (cogeneration of electricity and heat). Both of these values are not measured within the conducted experimental campaign. The simplifications with regards to concept in Figure 2 are summarized as follows:

- 100 % of reforming occurs externally in the steam reformer, since the targeted steam-to-methane ratio ($\dot{n}_{H_2O}/\dot{n}_{CH_4}$) is 2.1 and a steam reformer outlet temperature (stream 3 in Figure 3) is 700 °C. However, the majority of the methane (on the order of 80 %) should be reformed internally to minimize the cathode fan power consumption (stream 31), and thus to maximize the system electrical net efficiency [12].

- During the startup phase of the SOFC system, water vapor can be supplied from an external source (electrical evaporator) to the steam

reformer (stream 22). However, the external steam is no longer necessary during operation with the AOR. A final version would need an internal water storage tank, which could be filled during nominal operation and an additional start-up burner, which can heat the SOFC stack and the evaporator during the startup procedure. The evaporator could supply steam to the steam reformer (stream not shown in Figure 2) until the AOR is sufficiently high.

- The FTU and the SOFC stack are placed in two separate electrical ovens (solid green lines) at different temperatures. The SOFC stack, fuel and air preheaters (stream 3 and 24, respectively), steam reformer, the burner, and the HEX downstream of the burner are in a hot box at 700 °C. The FTU and the recirculation ratio (RR) measurement devices (V1 and V2) are at 195 °C. The electricity of these two ceramic ovens (stream 30 and 32) would thus need to be account as auxiliary power to calculate the SOFC system electrical net efficiency. In a final realization, all previously mentioned components would be placed in an insulated hot box that is not actively heated.

- The SOFC stack has a gross DC power of 6 kW_{el}; however, the FTU was originally designed for a 10 kW_{el} system.

- The blade tip clearance in the AOR fan is 0.15 mm instead of the original design value of 0.05 mm for risk mitigation. The fan blade tip clearance has a significant impact on the achievable pressure rise at the design AOR mass flow rate (4.8 $kg\,h^{-1}$) [10].

- A manually-operated ball valve at the fan outlet prevents the fluid from

bypassing the SOFC stack, e.g., the flow direction of streams 7, 6, and 5 (in Figure 3) is reversed during the startup phase. This could be replaced with a more simple check valve in a final version.

- The anode off gas (stream 9) and the cathode off-gas (stream 25) are mixed in the burner; hence, the air-fuel equivalence ratio in the burner is much higher than the ideal value of 1.1. This leads to a lower water vapor molar fraction in the anode off-gas, to less condensed water, to a lower heat recovery in the condenser (stream 10), and thus to a lower utilization ratio. Keeping the stream 9 and 25 separate is thus favorable for increased condensation of water, increased utilization ratio and better control of the flame temperature [13]. Additionally, ambient air is mixed into the burner (stream 27) to control the burner outlet temperature to 730 °C.

- The non-recirculated anode off-gas (stream 8-11) is first condensed, burned, and recondensed. The reverse order (first burning and then condensing) reduces the heat losses of the HEXs.

- The cathode air mass flow rate is kept constant at $5.1\,\mathrm{kg\,h^{-1}}$ for all operating points. The electrical net efficiency is thus not optimized, since the mass flow rate, and thus the cathode fan power consumption (stream 31 in Figure 3) could be lowered for the off-design points.

- The evaporator is electrical (stream 29), and thus the FTU and the SOFC are not thermally coupled, i.e., the HEX downstream of the burner does not provide heat to the evaporator.

- The turbine and the SOFC water systems are not coupled. The pump draws deionized water from an external tank (stream 15 in Figure 3); hence, a water treatment system is not necessary. The expanded steam in the turbine leaves the system via chimney (stream 19). The condensed water from the SOFC system (stream 11 and stream 12) is sent to drain.

- Due to the proof-of-concept nature of the presented setup, no automation was included; hence, a constant on-site surveillance of the entire system is necessary.

Figure 4 shows a) a digital image of the oven that contains the FTU, b) a digital image of the two Venturi nozzles that measure the RR, and c) a photo of the implemented FTU test rig without the oven cover.

Anode off-gas cooling: On the anode side, the off-gas exits the SOFC at a temperature of up to 800 °C. Since the FTU is designed for an operational temperature of 200 °C, an HEX precools the off-gas (stream 4, not shown in Figure 3) with ambient air to 200 °C. The off-gas is then conducted to the fan inlet in corrugated pipes that are exposed to the FTU oven atmosphere, thus adapting the gas temperature to the FTU temperature. A constant temperature at the fan inlet is guaranteed, favoring stable operation of the FTU.

Measurement of the RR: Downstream of this anode outlet HEX, the off-gas enters a custom-made double Venturi nozzle in accordance with ISO 5167-4 norm [14], as shown in Figure 4 b). The entrance is stream 4 (anode off-gas), the exit to the burner is stream 8, and the exit to the AOR fan is stream 5. Thus, the burner mass flow rate is measured in the Venturi 1 (V1)

and the AOR mass flow rate in Venturi 2 (V2) as shown in Figure 3. This design is advantageous, since the temperature, pressure, and gas composition, and thus the density is in both Venturi nozzles identical. Therefore, the RR is a function of the Venturi nozzle differential pressures (Δp) between the static pressure measurement at the inlet and at the throat pressure tap (+ and -, respectively, in Figure 4 b). Thus, the discharge coefficient (CD) is a function of the Reynolds number based on the throat hydraulic diameter (Re_{d_h}),

$$RR = \frac{\dot{n}_5}{\dot{n}_4} = \frac{1}{\frac{CD_{V1}\left(Re_{d_h,V1}\right)}{CD_{V2}\left(Re_{d_h,V2}\right)}\sqrt{\frac{\Delta p_{V1}}{\Delta p_{V2}}} + 1} \tag{1}$$

assuming a similar fluid density and geometry for both Venturi nozzles. A 1.5 mm diameter k-type thermocouple (red point in Figure 4 b) measures the fluid temperature downstream of Venturi nozzle 1. The pressure tap at the nozzle throat (- in Figure 4 c) measures the differential pressure with respect to the ambient. With these two variables and the ambient pressure, it is possible to calculate the fluid density, viscosity, and velocity, to compute the Reynolds numbers and the discharge coefficients (CD_{V1} and CD_{V2}). However, the exact fluid composition remains unclear and is estimated with an SOFC stack model and the respective measured variables. According to the ISO 5167-4 norm [14], the Venturi nozzle discharge coefficient is constant for high Reynolds numbers (above 2×10^5). However, for lower Reynolds numbers, it drops with decreasing Reynolds number. Since the Re_{d_h} may drop significantly below 15 000 during the tests, which strongly affects the discharge coefficient, and due to the fact that the Venturi nozzle area deviates from the norm, the nozzles were calibrated in-house.

Valve at fan outlet: In order to prevent the fluid from bypassing the SOFC stack if the FTU is not operational, the fan outlet features a ball valve that is closed during SOFC startup (see ball valve in Figure 3). Once the SOFC stack reached nominal operation, the FTU starts (with a closed valve at the fan outlet) and rises the pressure at the fan outlet above the reformer inlet pressure. The valve is then opened and the FTU begins to recirculate the anode off-gas. The initial water vapor supply to the reformer (stream 22 in Figure 3) is decreased and the AOR increased gradually until the reformer water vapor supply can be turned off and the stack operates with the AOR exclusively.

Measurement of efficiency and power: Due to risk mitigation (leakage of CO), it is not possible to use polytetrafluoroethylene (PTFE) tubing at the fan and the turbine outlet to thermally insulate the FTU. Hence, a reliable measurement of the turbine and fan powers, as well as the efficiencies by measuring the respective inlet and outlet temperatures, as well as the respective inlet mass flow rate was not possible, due to increased heat conduction from the oven to the environment [10].

4. Results and analysis

The steam-driven FTU was successfully coupled with a $6\,\mathrm{kW_{el}}$ SOFC provided by the company SOLIDpower. Electrical gross DC efficiencies,

$$\eta_{el,gross} = \frac{P_e}{\dot{n}_{fuel,1} LHV_{fuel}} \tag{2}$$

based on the LHV, of 66 % in part load ($4.5\,\mathrm{kW_{el}}$) and 61 % in full load ($6.4\,\mathrm{kW_{el}}$) for a global FU of 85 % were obtained. The global FU, referred to

as the FU in this paper, was measured.

$$f_{u,global} = \frac{\dot{n}_{fuel,1} - \dot{n}_{fuel,8}}{\dot{n}_{fuel,1}} = \frac{I}{z_e \boldsymbol{F}} \frac{z_{layer} M_{fuel}}{\dot{m}_{fuel,1}} \tag{3}$$

It corresponds to the fraction of the fuel molar flow rate that reacted within the SOFC system; i.e., the difference between the fuel in stream 1 and stream 8 in Figure 3 ($\dot{n}_{fuel,1} - \dot{n}_{fuel,8}$) to the fuel molar flow rate at the system inlet ($\dot{n}_{fuel,1}$). It is controlled with the SOFC load and it is measured with the SOFC current (I) and the fuel mass flow rate ($\dot{m}_{fuel,1}$), assuming steam reforming of methane ($z_e = 8$) and a stack with 60 layers ($z_{layer} = 60$). The local FU is a function of the measured global FU in eq. (3) and of the measured RR in eq. (1).

$$f_{u,local} = f_{u,global} \frac{1 - RR}{1 - RR f_{u,global}} \tag{4}$$

The turbine steam molar flow rate ($\dot{n}_{15}$, stream 15 in Figure 3 and Figure 2) is measured within the experiments. The anode off-gas (stream 8 in Figure 3 and Figure 2) contains water vapor, as well as unused hydrogen. Thus, the maximum molar flow rate of condensable water vapor

$$\dot{n}_{water} = 2\dot{n}_{fuel,1} \tag{5}$$

is a function of the fuel molar flow rate ($\dot{n}_{fuel,1}$), assuming methane as fuel, 100 % efficiency of the burner, and full condensation of the anode off-gas. The excess water ratio (EWR)

$$EWR = \frac{\dot{n}_{water}}{\dot{n}_{15}} \tag{6}$$

is an indicator, whether enough water is available in the anode off-gas to propel the turbine. As a result, there are three different cases, depending on

the theoretical maximum molar flow rate of condensable water vapor ($\dot{n}_{water}$) in eq. (5) and the measured steam molar flow rate through the turbine ($\dot{n}_{15}$).

- $EWR > 1$: The steam molar flow rate through the turbine is lower than the maximum molar flow rate of condensable water vapor. Thus, no water vapor needs to be recirculated to the condenser (stream 20 in Figure 2 is zero) and the entire water vapor leaves the system at stream 21. The water recirculation ratio ($RR_{water} = \dot{n}_{15}/\dot{n}_{12}$) is the ratio of the molar flow rate of stream 15 to stream 12 (both in Figure 2) therefore is smaller than 1. Thus, some water leaves the system at stream 13.

- $EWR = 1$: Both the stream 13 and 20 in Figure 2 are zero, i.e. the condensed water within the system is equal to the turbine steam molar flow rate.

- $EWR < 1$: The steam molar flow rate through the turbine is higher than $\dot{n}_{water}$; hence, part of the steam through the turbine needs to be recirculated. The steam recirculation ratio ($RR_{steam} = \dot{n}_{20}/\dot{n}_{19}$) is the ratio of the molar flow rate of stream 20 to stream 19 (both in Figure 2) is thus greater than 0.

Cell potential: Figure 5 shows the measured cell potentials and the current of the 6 kW_{el} SOFC stack at the design-point with four different global FUs. The four numbers (①, ②, ③, and ④) in Figure 5 correspond to the four experiments listed in Table 2 (experiment number 1, 2, 3, and 4). The global FU corresponds tp 0.7, 0.75, 0.8, and 0.85, respectively. The six cell potential curves were obtained from six different measurement locations

in the stack, each averaged over 10 cells (total cell number is 60). During experiment 1 (global FU of 0.7), the difference between the maximum measured cell potential (0.819 V) and the minimum measured cell potential (0.807 V) was 0.012 V, suggesting a homogeneous distribution of the fuel and similar cell efficiencies. The cell voltage efficiency (cell potential divided by the reversible potential) was 79 % and 78 %, respectively, at this operational point. The cell potential dropped to 0.769 V and 0.737 V, respectively, for experiment 4 (global FU of 0.85). This is equal to a cell voltage efficiency of 74 % and 71 %, respectively. Since the difference between the maximum and minium cell potential (0.032 V) was relatively high at this operational point, the SOFC stack was only operated for several minutes at a global FU of 0.85. In order to protect the prototype SOFC stack, a global FU higher than 0.85 was not investigated.

Coupling procedure: Table 1 represents the evolution of the results during the transition phase of the coupling procedure between the FTU and the SOFC stack. During the first experiment (c0), the steam for the reforming process was supplied from an external electrical evaporator (stream 22 in Figure 3). During the coupling process, the methane mass flow rate was maintained at 0.74 kg h^{-1}. The steam-to-methane ratio ($\dot{n}_{H_2O}/\dot{n}_{CH_4}$) in stream 2 was 2.1 at this operational point, which was the targeted value during the coupling procedure (experiment c0). The external steam injection into the reformer was then gradually reduced from 1.74 kg h^{-1} to 0, while the RR was increased from 0 (c1) to 47 % (c12) to maintain the targeted steam-to-methane ratio of 2.1. This RR was realized with turbine steam mass flow

rates of 1.5 kg h^{-1} and 2 kg h^{-1}, respectively, which corresponded to turbine total-to-total pressure ratios of 1.50 and 1.84, respectively, and a shaft rotational speeds of 149 krpm and 170 krpm, respectively. The transition was performed through 12 discrete steps indicated with c1 to c12 in Table 1.

Before coupling the AOR fan with the stack (experiment c0), the fan outlet total pressure was adjusted to be slightly above the reformer inlet total pressure. After the valve was opened (ball valve in Figure 3), the AOR started, which resulted in a slight drop of the total-to-total fan pressure rise from 51 mbar (experiment c0) to 47 mbar (c1). Since the anode mass flow rate increased with increasing RR, the fan total-to-total pressrue rise increased from 47 mbar (experiment c1) up to 62 mbar (c10). For the last three coupling steps (experiments c10, c11, and c12), the turbine inlet steam mass flow rate was constant (1.98 kg h^{-1}). The anode off-gas mass flow rate decreased from 4.85 kg h^{-1} (experiment c10) to 4.68 kg h^{-1} (c12); hence, the fan total-to-total pressure rises decreased from 62 mbar (c10) to 59 mbar (c12).

The cathode air mass flow rate was kept constant at 5.1 kg h^{-1} for all experiments (Tables 1 and 2), corresponding to an excess air ratio (EAR) of 4.4 for the coupling procedure (methane mass flow rate of 0.74 kg h^{-1}). The auxiliary powers (P_{aux}, e.g., the cathode fan electrical power) was not measured. Thus, a calculation of the electrical net efficiencies was not possible and Tables 1 and 2 only present the electrical gross DC efficiencies, as stated in eq. (2).

During the coupling procedure, the global FU was maintained at 0.7. Since the RR gradually increased, the local FU decreased from 0.7 (experiment c0) to 0.55 (c12). As a consequence, the mean cell voltages increased from

0.797 V (c0) to 0.813 V (c12); the electrical power output and the electrical gross DC efficiency increased by 0.12 kW_{el} and 1.15 percentage points, respectively.

Table 1 also lists the EWR as defined in eqs. (5) and (6). For experiment c0 to c4, the EWR is above 1, suggesting that theoretically enough water vapor is available in the anode off-gas. However, the actual available water vapor is lower, since the burner has an efficiency lower than 100 % and a fraction of the water vapor can not be condensed. This depends on the anode off-gas composition (e.g., EAR in the burner) and on the condensing temperature. In the final system, the actual EWR would therefore be lower. For experiment c5 to c12, part of the turbine exhaust needs to be recirculated to the condenser, as indicated by $RR_{steam} = 1 - EWR$.

Characterization: Figure 6 and Table 2 summarize the characterization of the 6 kW_{el} SOFC stack coupled to the steam-driven AOR fan. Each number in Figure 6 corresponds to an experiment listed in Table 2. The system was characterized at different loads, corresponding to different methane mass flow rates.

- 100 % load (0.74 $kg\,h^{-1}$): experiment 1-4
- 92 % load (0.68 $kg\,h^{-1}$): experiment 5-10
- 66.7 % load (0.50 $kg\,h^{-1}$): experiment 11-14
- 50 % load (0.37 $kg\,h^{-1}$): experiment 15-18

The power densities at 92 % load correspond to the power density of the BlueGEN produced by SOLIDpower (0.40 $A\,cm^{-2}$). For each load case, four

different global FUs (i.e., 0.7, 0.75, 0.8, and 0.85) were investigated. The turbine inlet temperature was maintained constant (215 °C ± 5 °C), as well as the fan inlet temperature (195 °C ± 5 °C). The turbine steam mass flow rate was fixed at 1.98 kg h^{-1}, 1.74 kg h^{-1}, 1.50 kg h^{-1}, and 1.38 kg h^{-1} for the 100 %, 92 %, 66.7 %, and 50 % load cases, respectively. For the 92 % load case, turbine steam mass flow rates of 1.98 kg h^{-1} (FU of 0.7, 0.75, 0.8, and 0.85) and 1.74 kg h^{-1} (FU of 0.8 and 0.85) were investigated. The resulting RR as stated in Equation (1) is therefore not constant. It generally increases with increasing global FU, while the load, i.e., the fuel mass flow rate, is constant. It varies between 0.42 (experiment 11 in Figure 6 and Table 2) and 0.51 (experiment 8). A higher RR leads to a higher dilution of the anode inlet gas, to a lower cell Nernst potential, and thus to a lower system efficiency. The RR of experiment 7 and 8 is 0.51. It decreased to 0.44 and 0.45 for the experiment 9 and 10, respectively. This leads to an increased electrical gross DC efficiency of 61.2 % and 63.0 %, respectively, as shown with the two blue up-pointing triangles in Figure 6. This is equal to an efficiency increase of 0.7 and 0.6 percentage points, respectively, compared to the two experiments with a RR of 0.51 (blue down-pointing triangles in Figure 6, numbered 7 and 8). The RR has therefore an impact on the SOFC system efficiency and power.

The water vapor molar ratio in the anode off-gas, and thus the anode off-gas density increases with increasing FU. The fan pressure rise increases for higher fluid densities, or the fan rotational speed decreases if the pressure rise is constant, but the fluid density increases. Thus, the shaft rotational

speed decreased with increasing FU, although the anode pressure loss, and thus the fan pressure rise increased with increasing FU. A high FU therefore is suggested to decrease the fan power. However, an accurate fan and turbine power measurement was not possible, since an insulation of the measurements section with PTFE tubes was not implemented, to mitigate the the risk of potential leakage of CO.
For a global FU of 0.85, electrical gross DC efficiencies of 61.4 %, 63.0 %, 65.8 %, and 66.9 % were reached for the 100 %, 92 %, 66.7 %, and 50 % load cases, respectively. This corresponds to a current density of 0.44 A cm^{-2}, 0.40 A cm^{-2}, 0.29 A cm^{-2}, and 0.22 A cm^{-2}, respectively. Considering a second-order extrapolation for a global FU of 92.5 %, an electrical gross DC efficiency of 65 % could be obtained for the 0.4 A cm^{-2} case.

For all the investigated operational points, EWR was below than 1, suggesting that the condensed water of the burner off-gas is not sufficient to drive the steam turbine. The EWR decreased from full load (0.84) to partial load (0.61), since the fuel inlet molar flow rate and thus the condensed water molar flow rate in the anode off-gas decreased. For all the experiments (1-18), part of the turbine exhaust would need to be recirculated to the condenser (stream 20 in Figure 2), as indicated by $RR_{steam} = 1 - EWR$.

Comparison to the stack without AOR: The SOFC stack was characterized at full load (fuel mass flow rate of 0.74 kg h^{-1}) and for a global FU of 0 to 75 % without AOR (Figure 7). The point with a FU of 0.75 is marked with A in Figure 7. The operating point with AOR at full load and a global

FU of 75 % corresponds to experiment 2 in Table 2 and to the point marked with 2 in Figure 7. Thanks to the thermally-driven AOR fan, the electrical gross DC efficiency (based on the LHV) was improved from 52.2 % to 57.3 % with the AOR, while the local FU from 75 % to 61 %, suggesting a higher SOFC stack lifetime.

5. Conclusion

A novel AOR fan was designed, manufactured, and experimentally coupled to a 6 kW_{el} SOFC system. This fan uses dynamic steam-lubricated bearings, more specifically herringbone-grooved journal and spiral-grooved thrust bearings that have proven to be reliable, even at temperatures up to 220 °C. Due to the high rotational speeds, the fan performance corresponds to the specified values, although the size is out of the common. The AOR is driven by a small-scale, partial-admission (21 %), and low-reaction (13 %) steam turbine with a tip diameter of 15 mm, which allows for an explosion-proof operation. To the best of the authors' knowledge, this is the first proof-of-concept of such a steam-driven AOR fan.

For a global FU of 75 % and a constant fuel mass flow rate, the electrical gross DC efficiency based on the LHV was improved from 52 % to 57 % with the AOR, while the local FU decreased from 75 % to 61 %, which is expected to significantly increase stack lifetime. For a global FU of 85 %, gross efficiencies of 66 % in part load (4.5 kW_{el}) and 61 % in full load (6.3 kW_{el}) were achieved with the AOR.

For the first proof-of-concept, the FTU and the SOFC system were decoupled in terms of thermal and water management. A preliminary investigation in-

dicates that the water content in the anode off-gas is at least 16 %, 12 %, and 26 % too low for the 100 %, 92 %, and 66.7 % load cases, respectively. Part of the turbine exhaust (at least 16 %, 12 %, and 26 %, respectively) therefore needs to be reused in the evaporator that provides the steam to the turbine. In a next step, the authors will decrease the AOR fan tip clearance from the current 0.15 mm to 0.05 mm, which increases the fan efficiency and therefore reduces the steam consumption of the turbine. Another way to decrase the steam consumption is by increasing the turbine inlet temperature. In a future project, the authors want to upscale the FTU and couple the SOFC and the FTU systems completely in terms of water and thermal management.

6. Acknowledgment

The authors acknowledge the research grant from the Canton de Vaud under the “100 millions de francs pour les énergies renouvelables et l’efficacité énérgetique”.

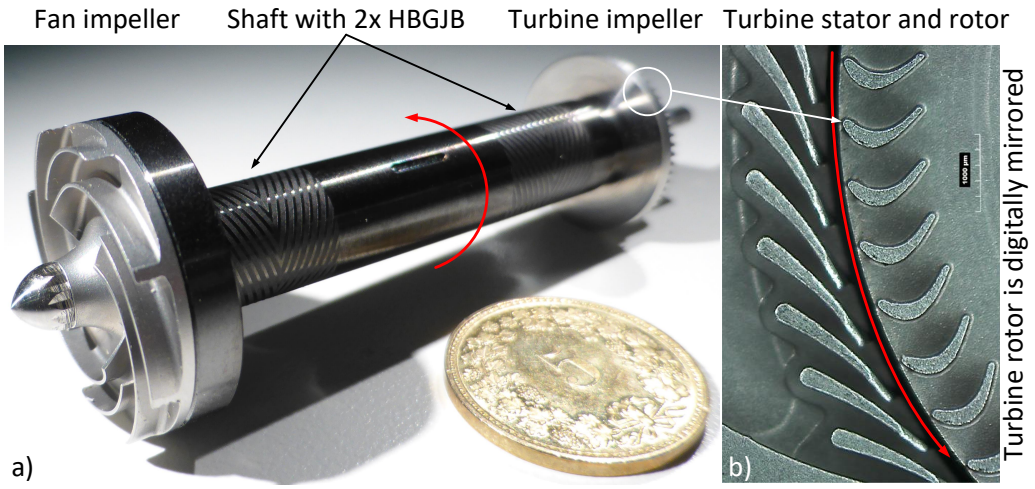

Figure 1: a) The fan-turbine unit with the radial fan impeller (left side), the shaft with diamond-like carbon coating and two herringbone-grooved journal bearings (HBGJBs), the radial-inflow turbine (right), and a comparison to a Swiss five centime coin (diameter at 17 mm). The direction of rotation is shown with a red arrow in figure a) and b). Figure b) shows a microscopic zoom of the the turbine rotor and stator blades (radial blade chord of 1 mm). The turbine blades are digitally mirrored, since turbine rotor and stator are normally mounted facing opposites directions.

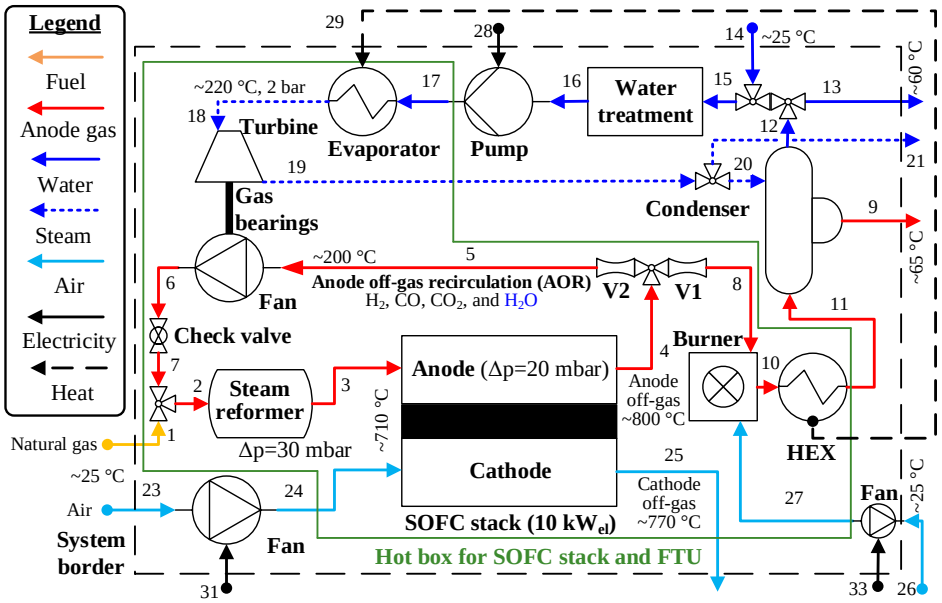

Figure 2: Novel SOFC system with steam-driven anode off-gas recirculation unit.

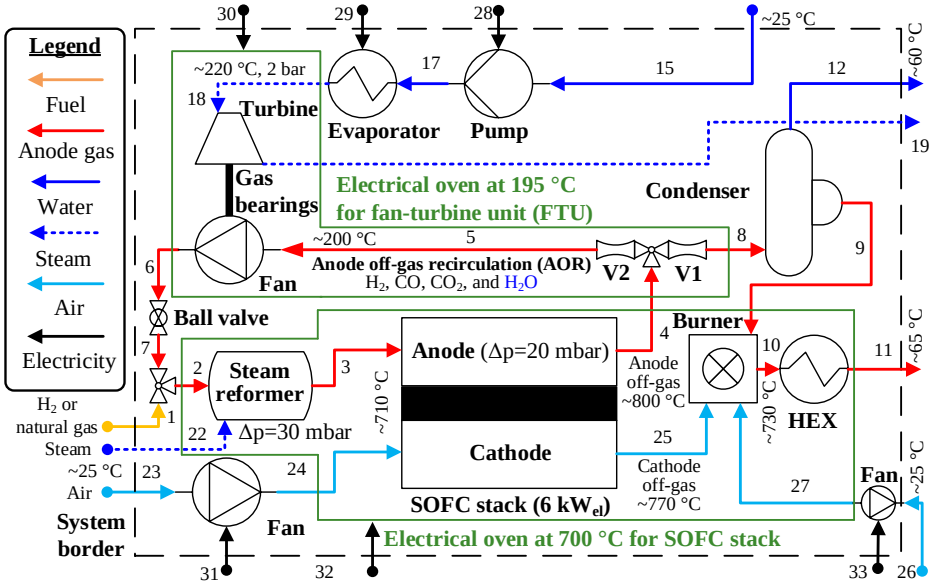

Figure 3: Realized SOFC system with steam-driven anode off-gas recirculation unit.

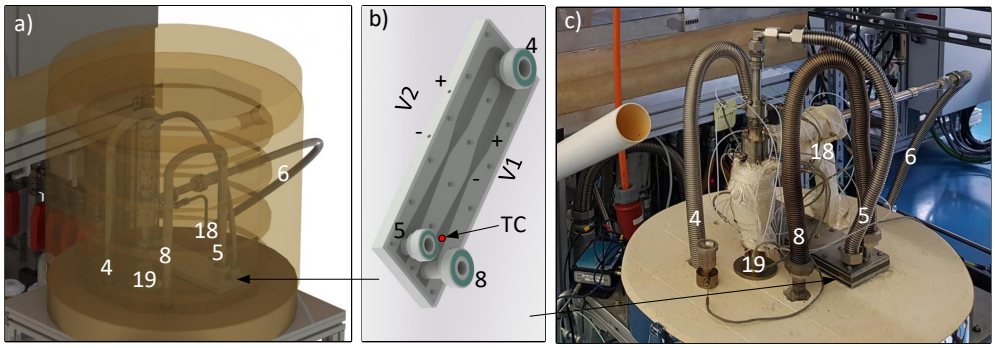

Figure 4: FTU test rig coupled with the SOFC: a) a digital image with mounted oven, b) the two Venturi nozzles for the recirculation rate measurement, and c) a photo with unmounted oven for the FTU test rig section.

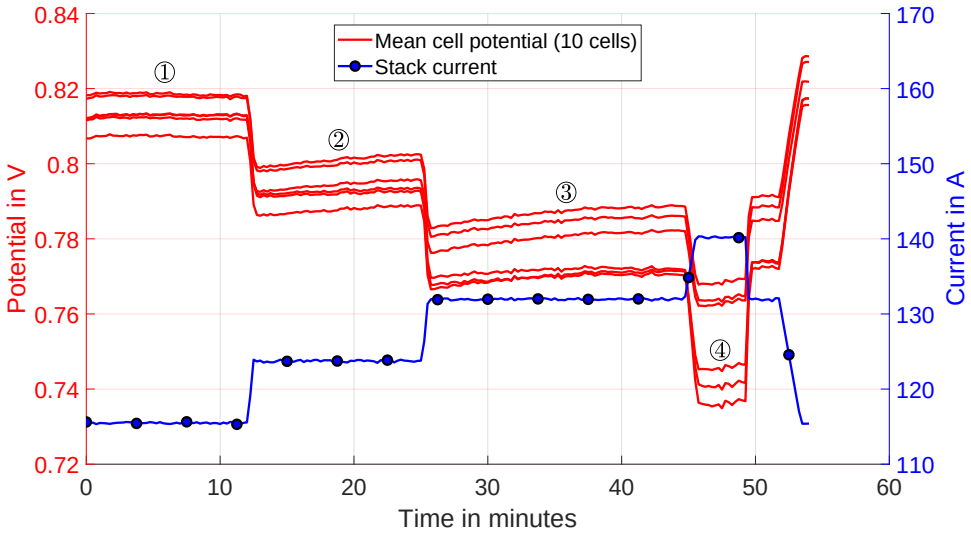

Figure 5: Measured cell potentials and total stack current for four experiments (1-4, as listed in Table 2).

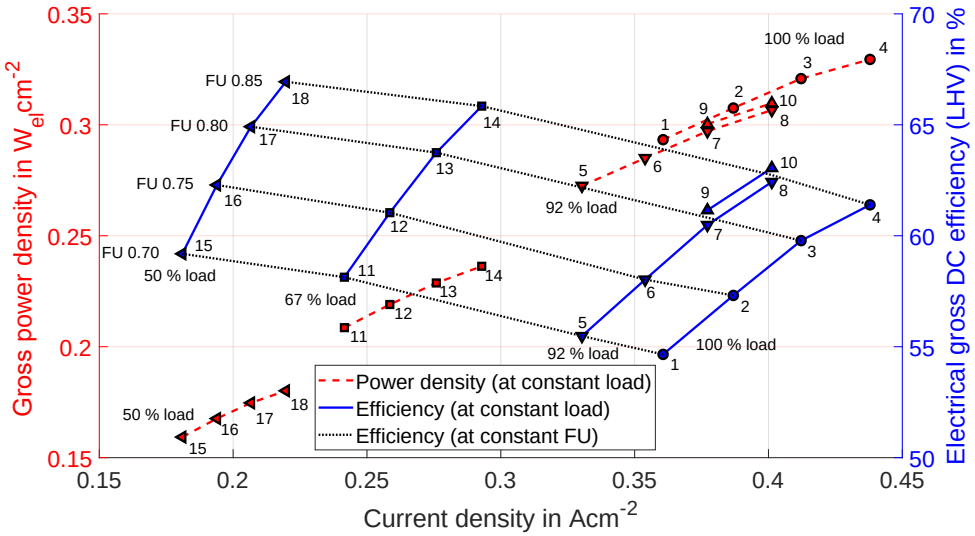

Figure 6: Electrical gross power density (60x4x80 cm^2 cells = 19 200 cm^2) and electrical gross DC efficiency based on the fuel lower heating value (LHV) for different global fuel utilization (0.85, 0.8, 0.75, and 0.70) and different loads (100 %, 92 %, 67 %, and 50 %) that correspond to different fuel mass flow rates for a system with a thermally-driven anode off-gas recirculation fan (recirculation ratios between 0.42-0.51). The numbers 1-18 correspond to the experiments in Table 2.

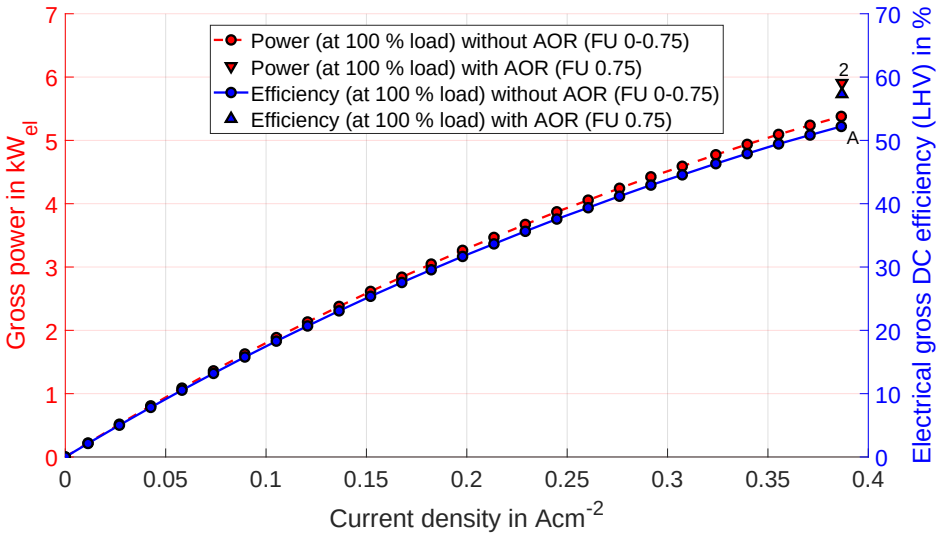

Figure 7: Electrical gross power and electrical gross DC efficiency based on the fuel lower heating value (LHV) for global fuel utilization (FUs) from 0 to 0.75 at full load that corresponds to fuel mass flow rates of $0.74\,\mathrm{kg\,h^{-1}}$ without anode off-gas recirculation (AOR). Comparison of the point A to a system with a thermally-driven AOR fan (FU of 0.75 and fuel mass flow rate of $0.74\,\mathrm{kg\,h^{-1}}$), which corresponds to the experiment 2 in Table 2.

Table 1: Coupling process of the FTU (steam-driven) with a 6 kW_{el} SOFC stack (60x4x80 cm^2 cells). The cathode air mass flow rate was maintained at 5.1 $kg\,h^{-1}$. The global fuel utilization was constant at 0.7. The turbine and fan inlet total temperatures were maintained at 215 °C ± 5 °C and at 195 °C ± 5 °C, respectively. The injected steam to the reformer was gradually replaced by anode off-gas recirculation.

Exp.	$\dot{m}$ **CH_4** **$kg\,h^{-1}$**	$\dot{m}^{g}$ **H_2O** **$kg\,h^{-1}$**	**FU**[a] **local** -	**RR** -	U **stack** **V**	I **stack** **A**	P_{el} **stack** **kW_{el}**	$\eta_{el,gross}$[b] **(DC LHV)** %	T^{c} **anode** °C	n_{rot} **shaft** **krpm**	$\dot{m}$ **turbine** **$kg\,h^{-1}$**	Π_{tt}[d] **turbine** -	$\dot{m}^{e}$ **fan** **$kg\,h^{-1}$**	Δp_{tt}[f] **fan** **mbar**	EWR[i]
c0	0.74	1.74	0.70	0.00	47.8	115.4	5.51	53.50	740.0	149.0	1.50	1.55	0.00	51	1.11
c1	0.74	1.74	0.69	0.04	47.6	115.4	5.50	53.34	740.0	149.0	1.50	1.54	0.16	47	1.11
c2	0.74	1.66	0.68	0.08	47.7	115.4	5.50	53.40	750.5	150.0	1.50	1.53	0.35	49	1.11
c3	0.74	1.50	0.67	0.13	47.7	115.4	5.51	53.47	752.5	152.0	1.56	1.54	0.58	50	1.07
c4	0.74	1.33	0.66	0.16	47.8	115.4	5.52	53.57	753.0	154.0	1.62	1.61	0.75	51	1.03
c5	0.74	1.16	0.65	0.21	47.9	115.4	5.53	53.69	753.5	156.5	1.68	1.66	1.00	53	0.99
c6	0.74	1.00	0.63	0.26	48.1	115.4	5.55	53.83	753.5	161.7	1.74	1.70	1.23	56	0.96
c7	0.74	0.83	0.62	0.30	48.2	115.4	5.56	53.93	753.5	163.0	1.80	1.73	1.40	57	0.93
c8	0.74	0.67	0.62	0.31	48.3	115.4	5.57	54.04	753.0	166.2	1.86	1.77	1.44	58	0.90
c9	0.74	0.50	0.59	0.39	48.3	115.4	5.57	53.93	752.0	170.7	1.92	1.81	1.86	60	0.87
c10	0.74	0.33	0.57	0.42	48.3	115.4	5.58	54.14	752.0	173.3	1.98	1.86	2.05	62	0.84
c11	0.74	0.17	0.57	0.44	48.6	115.4	5.61	54.41	751.0	170.7	1.98	1.85	2.10	60	0.84
c12[h]	0.74	0.00	0.55	0.47	48.8	115.4	5.63	54.65	750.0	169.8	1.98	1.84	2.21	59	0.84

[a] Calculated with eq. (4)

[b] Caclulated with eq. (2)

[c] Mean anode temperature. The anode and cathode inlet temperatures were maintained at 710 °C ± 1 °C

[d] Measured between turbine inlet and outlet

[e] Mass flow rate calculation based on the estimated anode off-gas composition. The exact gas composition was not measured

[f] Measured between fan inlet and outlet

[g] Injected in the reformer for the steam reforming process

[h] Experiment c12 is equal to experiment 1 in Table 2

[i] According to eq. (6)

Table 2: $6\,kW_{el}$ SOFC stack ($60x4x80\,cm^2$ cells) with anode off-gas recirculation (FTU, steam-driven). The cathode air mass flow rate was maintained at $5.1\,kg\,h^{-1}$. The turbine and fan inlet total temperatures were maintained at $215\,°C \pm 5\,°C$ and at $195\,°C \pm 5\,°C$, respectively.

Exp.	$\dot{m}$ **CH_4** $kg\,h^{-1}$	**FU global** -	**FU**[a] **local** -	**RR** -	U **stack V**	I **stack A**	P_{el} **stack** kW_{el}	$\eta_{el,gross}$[b] **(DC LHV)** %	T[c] **anode** °C	n_{rot} **shaft** krpm	$\dot{m}$ **turbine** $kg\,h^{-1}$	Π_{tt}[d] **turbine** -	$\dot{m}$[e] **fan** $kg\,h^{-1}$	Δp_{tt}[f] **fan** mbar	EWR[i]
1	0.74	0.7	0.55	0.47	48.8	115.4	5.6	54.7	750	169.8	1.98	1.84	2.21	59	0.84
2	0.74	0.75	0.61	0.48	47.7	123.8	5.9	57.3	750	169.4	1.98	1.84	2.35	62	0.84
3	0.74	0.8	0.67	0.48	46.7	131.9	6.2	59.8	755	168.0	1.98	1.84	2.46	64	0.84
4	0.74	0.85	0.75	0.48	45.1	140.1	6.3	61.4	756.5	165.5	1.98	1.83	2.54	65	0.84
5	0.68	0.7	0.54	0.50	49.5	105.7	5.2	55.5	751.5	170.9	1.98	1.83	2.32	60	0.77
6	0.68	0.75	0.60	0.50	48.3	113.3	5.5	58.0	749.5	169.2	1.98	1.83	2.41	61	0.77
7	0.68	0.8	0.66	0.51	47.3	120.7	5.7	60.5	748.5	166.5	1.98	1.83	2.50	62	0.77
8	0.68	0.85	0.74	0.51	45.9	128.4	5.9	62.4	748.5	164.6	1.98	1.83	2.55	63	0.77
9	0.68	0.8	0.69	0.44	47.8	120.7	5.8	61.2	752.5	149.7	1.74	1.73	2.02	51	0.88
10	0.68	0.85	0.76	0.45	46.3	128.4	5.9	63.0	753	148.2	1.74	1.73	2.06	53	0.88
11	0.50	0.7	0.57	0.42	51.8	77.3	4.0	58.1	733	130.8	1.50	1.57	1.38	37	0.74
12	0.50	0.75	0.62	0.45	50.8	82.7	4.2	61.0	732	129.2	1.50	1.57	1.61	37	0.74
13	0.50	0.8	0.69	0.46	49.7	88.3	4.4	63.7	732.5	128.7	1.50	1.57	1.69	39	0.74
14	0.50	0.85	0.75	0.46	48.4	93.7	4.5	65.8	733	128.1	1.50	1.57	1.74	39	0.74
15	0.37	0.7	0.55	0.47	52.8	57.9	3.1	59.2	734.5	116.4	1.38	1.51	1.40	31	0.61
16	0.37	0.75	0.61	0.48	51.9	62.1	3.2	62.3	735.5	115.7	1.38	1.51	1.47	31	0.61
17	0.37	0.8	0.67	0.48	50.7	66.1	3.4	64.9	736	115.5	1.38	1.51	1.50	32	0.61
18	0.37	0.85	0.75	0.48	49.2	70.3	3.5	66.9	737.5	115.2	1.38	1.51	1.57	32	0.61

[a] Calculated with eq. (4)

[b] Caclulated with eq. (2)

[c] Mean anode temperature. The anode and cathode inlet temperatures were maintained at $710\,°C \pm 1\,°C$

[d] Measured between turbine inlet and outlet

[e] Mass flow rate calculation based on the estimated anode off-gas composition. The exact gas composition was not measured

[f] Measured between fan inlet and outlet

[i] According to eq. (6)

List of Acronyms

AOR	anode off-gas recirculation
DC	direct current
DLC	diamond-like carbon
EAR	excess air ratio
EWR	excess water ratio
FTU	fan-turbine unit
FU	fuel utilization
HEX	heat exchanger
LHV	lower heating value
PTFE	polytetrafluoroethylene
RR	recirculation ratio
SOFC	solid oxide fuel cell

Nomenclature

Greek Symbols

η	efficiency
Π	Pressure ratio

Roman Symbols

CD	Discharge coefficient
EWR	Excess water ratio
$\boldsymbol{F}$	Faraday constant ($96\,485.3329\,\mathrm{s\,A\,mol^{-1}}$)
f_u	Fuel utilization
I	Current in A
LHV	Lower heating value in $\mathrm{J\,mol^{-1}}$
M	Molar mass in $\mathrm{kg\,mol^{-1}}$
$\dot{m}$	Mass flow rate in $\mathrm{kg\,s^{-1}}$
$\dot{n}$	Molar flow rate in mol/s
n_{rot}	Rotational speed in krpm
P	Power in W
p	Pressure in bar
Re	Reynolds number

RR Recirculation ratio

T Temperature in °C

U Voltage in V

z_e Number of electrons

z_{layer} Number of cell layers in the SOFC stack

Subscripts

e electrical

h hydraulic

tt total-to-total

References

[1] M. Powell, K. Meinhardt, V. Sprenkle, L. Chick, G. McVay, Demonstration of a highly efficient solid oxide fuel cell power system using adiabatic steam reforming and anode gas recirculation, Journal of Power Sources 205 (2012) 377–384 (May 2012). doi:10.1016/j.jpowsour.2012.01.098.
URL http://www.sciencedirect.com/science/article/pii/S0378775312001991

[2] B. P. Borglum, H. Ghezel-Ayagh, Development of Solid Oxide Fuel Cells at Versa Power Systems and Fuel Cell Energy, ECS Transactions 57 (1) (2013) 61–66 (Oct. 2013). doi:10.1149/05701.0061ecst.
URL http://ecst.ecsdl.org/cgi/doi/10.1149/05701.0061ecst

[3] M. Halinen, A. Pohjoranta, L. Kujanp, V. Visnen, P. Salminen, Summary of the RealDemo project 2012-2014, Tech. rep., VTT Technical Research Centre of Finland (2014).

[4] R. Peters, M. Engelbracht, W. Tiedemann, I. Hoven, R. Deja, V. N. Nguyen, L. Blum, D. Stolten, Development and Test of a Solid Oxide Fuel Cell Subsystem with a Low Temperature Anode Off-Gas Recirculation, ECS Transactions 78 (1) (2017) 2489–2495 (May 2017). doi:10.1149/07801.2489ecst.
URL http://ecst.ecsdl.org/content/78/1/2489

[5] K. Weeber, P. Horstmann, J. Miersch, Changes in Power Generation and

Distribution and the role of SOFC, in: Proceedings of 13th European SOFC & SOE Forum 2018, 2018 (2018).

[6] Y. Tanaka, K. Sato, A. Yamamoto, T. Kato, Development of Anode Off-Gas Recycle Blowers for High Efficiency SOFC Systems, ECS Transactions 57 (1) (2013) 443–450 (Oct. 2013). doi:10.1149/05701.0443ecst.
URL http://ecst.ecsdl.org/content/57/1/443

[7] J. Rechberger, M. Reissig, M. Hauth, AVL SOFC Systems on the Way of Industrialization, ECS Transactions 57 (1) (2013) 141–148 (Oct. 2013). doi:10.1149/05701.0141ecst.
URL http://ecst.ecsdl.org/content/57/1/141

[8] G. Agrawal, Advances in Fuel Cell Blowers, Tech. rep., R&D Dynamics Corporation, www.netl.doe.gov/file%20library/events/2009/seca/presentations/Agrawal_Presentation.pdf, Accessed: 2015-04-14 (2010).

[9] H. Hooshang, High Temperature Anode Recycle Blower for Solid Oxide Fuel Cell, Tech. rep., Mohawk Innovative Technology, https://www.netl.doe.gov/research/coal/project-information/proj?k=FE0027895, Accessed: 2018-08-16 (2016).

[10] P. H. Wagner, Z. Wuillemin, S. Diethelm, J. Van herle, J. Schiffmann, Theoretical and Experimental Investigation of a Small-Scale, High-speed, and Oil-free Radial Anode Off-Gas Recirculation Fan for Solid Oxide Fuel Cell Systems, in: ASME Turbo Expo 2019: Turbomachinery Technical Conference and Exposition, 2019 (2019).

[11] P. H. Wagner, Integrated Design, Optimization, and Experimental Realization of a Steam-Driven Micro Recirculation Fan for Solid Oxide Fuel Cell Systems, PhD thesis, EPFL, Lausanne, thesis number 9337 (2019).

[12] P. H. Wagner, Z. Wuillemin, S. Diethelm, J. Van herle, J. Schiffmann, Modeling and Designing of a Radial Anode Off-Gas Recirculation Fan for Solid Oxide Fuel Cell Systems, Journal of Electrochemical Energy Conversion and Storage 14 (1) (2017) 011005–011005–12 (May 2017). doi:10.1115/1.4036401.
URL http://dx.doi.org/10.1115/1.4036401

[13] HTceramix S.A., WO 2016/087389 A1: SOFC system and method of operating a SOFC system, Patent, HTceramix S.A. (Jun. 2006).

[14] International Organization for Standardization (ISO), ISO 5167: Measurement of fluid flow by means of pressure differential devices inserted in circular cross-section conduits running full, Standard, ISO (Jun. 2003).